H-SAF Associate Scientist Activity

H_AS23_02

Final report

Title:

H SAF Precipitation Products Evaluation in Sub-Saharan Africa

December 2023

Kumah Kwabena Kingsley[1]

[1] Trans-African Hydro-Meteorological Observatory (TAHMO), Nairobi, Kenya

Contents

List of Figures

List of Tables

1.0 Introduction

In sub-Sahara Africa (SSA), agriculture is typically rainfed; for this reason, most farmers demand accurate rainfall onset-cessation information to plan land preparations for growing seasons [1, 2]. Additionally, temporally consistent rainfall records are essential for operational meteorology, identifying extreme events and assessing their associated risks, developing climate-informed early warning systems, planning, and research [3]. Unfortunately, using conventional rainfall monitoring systems such as rain gauges and weather radars for large-scale rainfall monitoring has proven expensive to establish and maintain, leading to critical gaps in current and historical ground rainfall data in SSA.

The fact that satellite-derived precipitation products provide spatiotemporally consistent and accessible data makes them beneficial for applications requiring rainfall information, provided their accuracy is well known. For this reason, several past studies have evaluated various satellite-derived rainfall products in SSA [4-6] to provide relevant feedback intended to improve the reliability of satellite rainfall products for many regional applications.

However, evaluation studies based on H SAF rainfall products are scanty, and their performances over the region are understudied despite their potential usage for many applications. Moreover, for the algorithm developers, the results of ground validation studies are helpful feedback for assessing product quality, benchmarking performance against existing datasets and previous versions, providing insights into developing new satellite rainfall observation missions, and identifying surprising or unexpected results.

In this context, this Associate Scientist (AS) activity aims to evaluate the various H SAF precipitation products, H03B, H05B, H64, and H68, using data from a network of weather stations across southern, eastern and western SSA operated by the Trans-African Hydro-meteorological Observatory (TAHMO) [7] for a period between 2020-2022, focusing on two primary objectives:

1. to assess the H SAF precipitation products' accuracy at different temporal scales and intercompare their performances in the different SSA regions;
2. to assess the capability of the different H SAF precipitation products to detect and estimate extreme rainfall in SSA.

The precipitation products evaluated constitute H SAF's suit of precipitation retrieval algorithms [8], allowing for an evaluation of products and corresponding algorithms in a relatively new area providing new insights into how these algorithms perform. More recent precipitation products, such as the H60B and H61B, set to improve the H03B and H05B products, required fine-tuning that did not allow their inclusion in this evaluation study at the beginning of this AS activity. Nevertheless, when available, this study's evaluation methods and techniques apply to new datasets.

Additionally, one innovative objective of this AS activity was to investigate the potential of using precipitation estimates derived from commercial microwave links (CML), the infrastructure used by telecom operators for data transmission on, e.g. mobile phones and television, for evaluating the H SAF precipitation products, with a specific focus area in Ghana where the CML data would be acquired. Unfortunately, though the AS established a data-sharing agreement with a telecom service provider in Ghana to use their data for precipitation retrieval, they couldn't provide reasonably archived (at least covering a rainy season period) and desirable temporal resolution CML data, preventing the fruition of this objective.

2.0 Study Area and Dataset

2.1 Study area

This study evaluated the H SAF precipitation products over SSA, divided into three broad regions: Southern (SA), Eastern (EA), and Western (WA) Africa (see Figure 1). Figure 1's bounding boxes do not

represent each region's geopolitical boundaries. They are used to evaluate the H SAF rainfall product performance under climatic conditions characterizing each region.

Variable rainfall regimes and patterns influenced by the Atlantic Ocean characterize the Western African climate. Additionally, the region's rainfall distribution may be linked to mesoscale convective systems and topography [9]. Abiodun, et al. [10] identified three climatic zones in this region. The Guinea coast – having a subhumid climate and an annual rainfall between 1250 and 1500 mm. A semi-arid Savannah zone with annual rainfall between 750 and 1250 mm. The Sahel zone, characterized by a distinctively unimodal short rainy season between June and September with an average annual rainfall of about 750 mm.

Eastern and Southern Africa rainfall is linked to the conditions of the Pacific Ocean. This region's high spatiotemporal rainfall variability is also linked to complex large-scale factors such as topography, lakes, and the intertropical convergence zone (ITCZ) [11, 12]. The rainfall distribution varies from month to month following the ITCZ movement. In the equatorial regions ($4^oS–7^oN$), rainfall is bimodal, consisting of long rainy (March–May) and short rainy (October–December) seasons. Above 7^oN, rainfall generally occurs between June and October, whereas in Southern Africa, it typically occurs between November and April [5, 12].
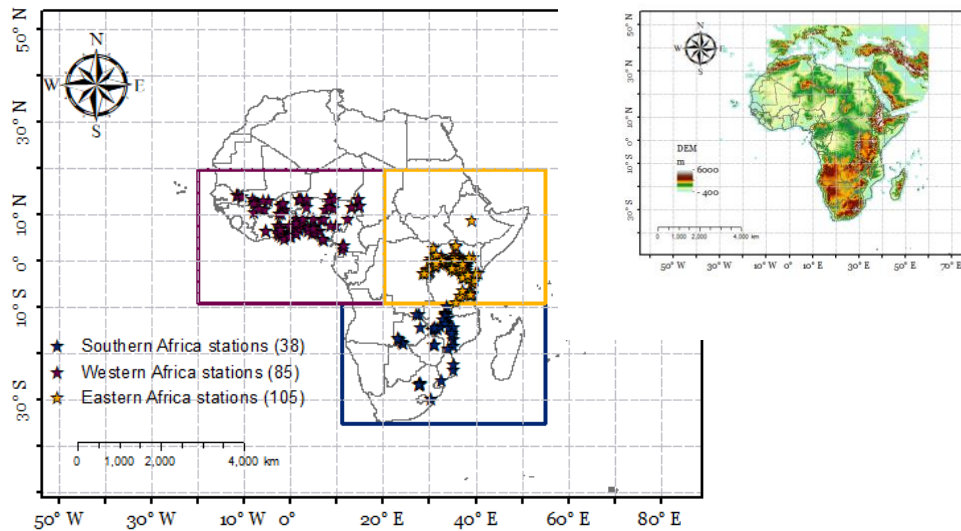
Figure 1 Study area showing the southern, eastern, and western SSA regions and the number of stations used in each region. The map insert is the topography of the study area based on ALOS DEM.

2.2 Dataset

This study evaluated the H SAF rainfall products using TAHMO's rain gauge data for the areas shown in Figure 1 from 2020 to 2022 with temporally consistent gauge and satellite data.

2.2.1 TAHMO

Over 200 TAHMO [7] weather stations (Figure 1) provided ground-based precipitation data that served as this study's reference data. TAHMO weather stations are ATMOS 41 model manufactured by the METER Group, equipped with precipitation, temperature, atmospheric pressure, relative humidity, solar radiation, wind speed, and wind direction sensors. The precipitation sensor relies on an electric drip counter, and several stations have ECRN-100 tipping-bucket rainfall sensors for cross-validation [5]. The rainfall data have a resolution of 0.0017 mm and an accuracy of 65% of measurement for rainfall between 0 and 50 mm (https://tahmo.org/technical-information/). TAHMO data are quality-

controlled by cross-calibration and comparison with nearby sensors, as well as qualitative comparison with satellite observations [7]. TAHMO stations have a 5-minute measurement interval of meteorological variables [2]. Only quality-controlled stations that have also been manually checked were used in this study. This study aggregated TAHMO's precipitation data to sub-daily, daily, dekadal, and monthly estimates.

2.2.2 H SAF

The H SAF rainfall products used in this study have characteristics that make them ideal for applications in SSA. For instance, the temporal (sub-hourly to daily) and spatial (3 to 25 km) resolution is conducive for studying convective rainfall characterised by sudden and intense rainfall over a small area, often related to flash floods common to many regions in the SSA rainfall. Moreover, the data is open-source and widely available over the SSA region.

The H03B is a 15 min, 3 by 3 km (on the Sub Satellite Point, SSP) precipitation product developed using a Rapid Update (RU) algorithm, which relies on the [13] method. The idea is to blend GEO IR and LEO MW observations to exploit the advantage of each sensor to tackle the problem of spatiotemporally evolving precipitation characteristics in relation to satellite observation using statistical techniques. RU uses spatiotemporally collocated SEVIRI-based IR and MW observations to create histogram-based relationships that are updated when new IR and MW observations are available. This geo-locating histogram relationship is based on equally spaced 2.5° by 2.5° (lat-lon) boxes. The algorithm calibrates the IR observations using MW-based rain rates based on the good correlation between the IR and MW-based rain rates observations, which is ideal for convective rainfall but less reliable for non-convective rainfall.

The H05B product is a 3 by 3 km (at SSP) spatial resolution derived by time integration of frequent precipitation data (e.g., H03) acquired using the RU algorithm. The product is generated every 3 hours and distributed at synoptic hours (00, 03, 06, 09, 12, 15,18, 21). The periods of integrating blended MW and IR retrievals at 15-minute intervals are the previous 3, 6, 12, and 24 hours.

The H64 product is a gridded daily precipitation product generated by merging PMW precipitation estimates from the H-AUX-23 and H67 with soil moisture-derived estimates from the SM2RAIN [7] algorithm. Over oceans, the algorithm only relies on PMW estimates. It is worth stating that factors including frozen soils, highly vegetated areas, and complex topography affecting the input product's reliability impact the H64 product's quality. H64 has 0.25° by 0.25° spatial resolution.

H68 is a Level 3 half-hourly (gridded) MW-based product generated by exploiting the combination of passive microwave (PMW) Level 2 instantaneous precipitation rate products. Every 30 minutes, the algorithm matches all available overpasses at a given grid point by DMSP (SSMIS), Metop/NOAA (AMSU/MHS), GCOM-W1 (AMSR2), SNPP and NOAA-20 (ATMS) and GPM-Core Observatory (GMI), together with H01, H02B, H18 Level 2 operational products, and H-AUX-17 and H-AUX-20 auxiliary modules to provide the best instantaneous precipitation rate estimate at the grid point. The number of matchups from different LEO satellite platforms reduces rapidly towards low latitudes, resulting in few product sample sizes in the study area, particularly in southern Africa. The product has a 0.25° by 0.25° spatial resolution.

3.0 Methodology

3.1 Assessing the accuracy of the different H SAF rainfall products at different temporal scales

3.1.1 The temporal and spatial scale of the evaluation

This study evaluated the different H SAF products at sub-hourly, hourly, daily, dekadal, and monthly temporal scales, matching time scales commonly used in hydro-meteorological applications of rainfall data. For instance, hydro-meteorological applications of precipitation data focusing on flash floods require sub-hourly timescale data. Dekadal data may be enough for agricultural applications, while applications focusing on drought may need monthly to seasonal data.

3.1.2 On the spatiotemporal difference between gauge and satellite

One must consider the observational scale mismatch between the satellite (pixel) and ground (point) data. Past studies, including [2, 8], have used point-to-pixel and pixel-to-pixel approaches to compare a ground-based in situ rainfall observation to a gridded satellite observation. The former assumes that the satellite's observation is representative of the whole pixel and directly compares the satellite to the ground observation. In contrast, the latter grids the ground observations using geostatistical techniques to match the satellite's grid resolution.

This study used the point-to-pixel approach to compare the satellite and ground data, albeit the approach differed with the different products. For the SEVIRI-based products (H03B and H05B), this study compared the ground data to the satellite data retrieved from the neighborhoods of 3 by 3 pixels around the station pixel to account for the spatial mismatch between the gauge and satellite data due to, e.g., parallax effect. More precisely, the pixel value (within the station's 3 by 3 pixels neighborhood) with a minimum difference between the station's observations was compared. For the H64 and H68 products, this study compared the gauge data with the satellite data retrieved for the gauge pixel. However, regardless of the approach, this study retains the original gauge for comparison with the satellite data as opposed to other approaches that interpolate between stations, which could smoothen extreme values relevant to this study's rainfall detection and estimation statistics.

TAHMO station's latitude-longitude locations were converted to spatial points, which retrieved the satellite's pixel observations for each H SAF product at their native spatial and temporal resolution. The gauge accumulates precipitation at 5-minute intervals, whereas H03B and H68 products observe precipitation intensities (mm/h) at their respective temporal resolutions. Therefore, this study estimated accumulated precipitation from their observations. For H03B, the 15-minute instantaneous observations were divided by a factor of 4 to estimate its precipitation accumulation in 15 minutes. The H68's low sub-daily samples over the study area due to LEO observations did not allow for a fair sub-daily evaluation relative to the gauge. Thus, its evaluation was at the daily, dekadal, and monthly time scales. The mean of all H68 observations in a day multiplied by 24, estimated its daily precipitation accumulations. We ignored no data values in all computations.

Subsequently, the gauge observations at the station pixel were merged with the satellite data into a single data frame. Rows with no data values in the gauge or satellite data column were removed, resulting in only a spatiotemporally collocated gauge and satellite data. The data was then aggregated to this study's various temporal evaluation scales by summing the observations in each time interval. For the hourly and sub-hourly analysis, a timestamp is considered rainy if the precipitation value is greater or equal to 0.5 mm; otherwise, it is considered dry. A 1 mm threshold was used for the daily, dekadal, and monthly analysis. These thresholds were applied in categorical and quantitative evaluations of the H SAF rainfall products.

3.2 Assessing the capability of the H SAF products for extreme rainfall detection and estimation

This study evaluated the various H SAF rainfall products for extreme rainfall detection and estimation using their daily precipitation estimates in Section 3.1.2. As in the previous analysis in Section 3.1.2, only spatiotemporally collocated gauge-satellite observations were used in this study. For a robust assessment, 3 indices were defined to indicate extreme precipitation: (1) daily precipitation exceeding 50 mm/day (Ext_{50}), (2) daily precipitation exceeding the 95th percentile of rainy days ($Ext_{95\%}$) and (3) daily precipitation exceeding the 99th percentile of rainy days ($Ext_{99\%}$), following previous studies' approach [14, 15].

Based on these indices, daily precipitation extremes were assembled from the spatiotemporally collocated gauge-satellite time series data to evaluate the satellite's extreme precipitation detection and estimation capabilities, focusing on 2 major questions below.
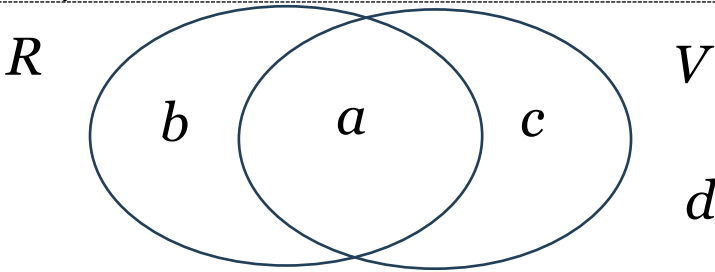
1. What is the range of extreme values detected and estimated by the gauge and satellite for a given extreme precipitation index?
2. What was the satellite's estimate when the gauge detected and estimated a precipitation value greater or equal to an extreme index?

The first question compares the satellite's extreme precipitation detections and estimates to the gauge to investigate its detectable range of extreme values. By contrast, the latter investigates the agreement between the gauge and satellite precipitation extremes.

3.4 The evaluation metrics

This study utilized standard categorical and quantitative metrics defined in Table 1 and several past studies [2, 16, 17]. All observations, including rain (wet) and no rain (dry), were used to compute these metrics. The probability of detection (POD), false alarm ratio (FAR), Bias, and critical success index (CSI) metrics evaluated the skill of the satellite data to detect rainfall.

Table 1 A summary of this study's evaluation metrics

Evaluation metric	Formula	Optimal value	Unit
POD	$\dfrac{a}{a+b}$	1	None
FAR	$\dfrac{c}{a+c}$	0	None
Bias	$\dfrac{a+c}{a+b}$	1	None
CSI	$\dfrac{a}{a+b+c}$	1	None
CC	$\dfrac{Cov(R,V)}{STD_R \times STD_V}$	1	None
MB	$\dfrac{\sum V - R}{\sum R}$	0	None
RMSE	$\sqrt{\left(\dfrac{1}{N}\right)\sum (R-V)^2}$	0	mm
KGE	$1 - \sqrt{(r-1)^2 + (\beta-1)^2 + (\gamma-1)^2}$ $\beta = \dfrac{\mu_V}{\mu_R}$ and $\gamma = \dfrac{CV_V}{CV_R} = \dfrac{\sigma_V/\mu_V}{\sigma_R/\mu_R}$	1	None

The μ, CV, and σ are the mean, coefficient of variation, and standard deviation, respectively.

All the categorical metrics were computed using *a, b, c,* and *d* elements, defined in the Venn diagram in Table 1. Assuming reference data R (herein TAHMO station observation) and the data to be validated V (herein H SAF rainfall), the element a constitutes all time intervals in which both R and V are considered as wet (i.e., the precipitation is above a certain threshold dependent on the temporal evaluation). The element b constitutes all wet intervals in R, where V is considered dry, and c is vice versa. The d element

is all intervals in which *R* and *V* are considered dry. Subsequently, the POD represents the fraction of *V*'s correct rainfall detection, and FAR is the fraction of wrong detections. Bias indicates if the *V* over or underestimates the number of observations in *R*, while the CSI represents the ratio of all events estimated and observed that are correctly detected.

The metrics: Pearson correlation coefficient (CC), mean relative bias (MB), root-mean-square error (RMSE), and the Kling-Gupta efficiency (KGE) [16, 18, 19] evaluated the satellite's skill in estimating rainfall amounts. CC shows the strength and direction of the linear relationship between *R* and *V*. MRB shows, on average, if *V* over or underestimates the *R* observations. RMSE quantifies the average difference between the *V* and *R* observations, providing more weight to large differences. KGE relies on correlation, bias, and variability terms to evaluate the satellite's precipitation estimation skill holistically. All observations, i.e., raining and non-raining, were used in computing these metrics.

4.0 Results and Discussion

4.1 Results

4.1.1 The H SAF products' accuracy at different spatiotemporal scales

Error! Reference source not found. Table 2 shows the descriptive statistics of each location's daily precipitation data and the count of wet and dry intervals. These statistics were computed from all station data combined (per location), thus representing statistics from a mixed space-time perspective. The data shows comparable mean and median daily precipitation values in SA, EA, and WA. Relatively higher standard deviation in SA and WA may, however, point towards high daily precipitation variability in these areas compared to EA. Overall, daily precipitation is often below 50 mm/day according to each location's 99 percentile value.

Table 2 Descriptive statistics of the reference data

Location	Mean	STD	50%	75%	99%	Wet count	Dry count
SA	2.17	9.13	0	0.12	40.91	8,609	45,819
EA	2.22	7.99	0	0.41	36.60	36,430	142,892
WA	2.18	8.91	0	0.08	41.57	21,083	113,823

50%, 75%, and 99% are 50th, 75th, and 99th percentile precipitation values in mm/day.

4.1.1.1 The sub-daily evaluation

Figure 2 shows the distribution of categorical metrics computed at each study location's station pixel to compare the H03B precipitation estimates to the station estimates at 30-minute intervals. The figure is analogous to Figure 3, which shows a similar distribution based on the quantitative metrics. The sub-daily categorical metrics were computed using a 0.5 mm threshold (see Section 3.1.2).
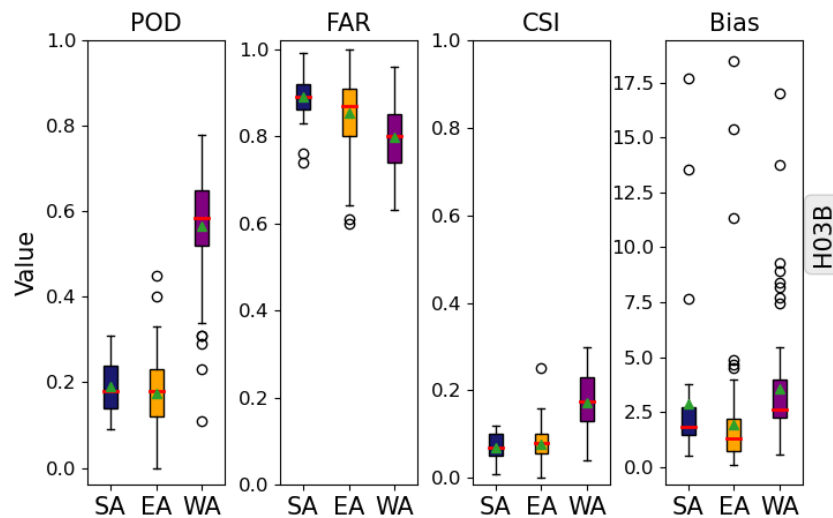

Figure 2 The distribution of categorical metrics computed at each study location's station pixel at 30-minute intervals. Boxes show the first, median (red lines), and third quartile. Whiskers (lines outside the box) extend

from the minimum to the first quartile and from the third quartile to the maximum; circles indicate outliers; green triangles are the average categorical metrics.

The metrics in Table 3 were computed based on a mixed space-time dataset constructed using the coincident satellite and gauge precipitation estimate observed at each study location's station pixel, providing H03B's average performance in each study location. Overall, the results show high FAR and Bias, coupled with low CSI regardless of location, pointing towards weak precipitation detection ability at 30-minute intervals relative to the station data. When comparing performance across locations, the POD and CSI suggest better performance in WA than in SA and EA (Figure 2 and Table 3).

H03B's quantitative precipitation estimation skill at 30-minute intervals is also weak, according to the KGE and CC values in Figure 3 and Table 3. Besides, all locations have a wet bias based on the above 0 MRB, especially in WA, while the average errors (RMSE) are comparable in WA and SA (Table 3).
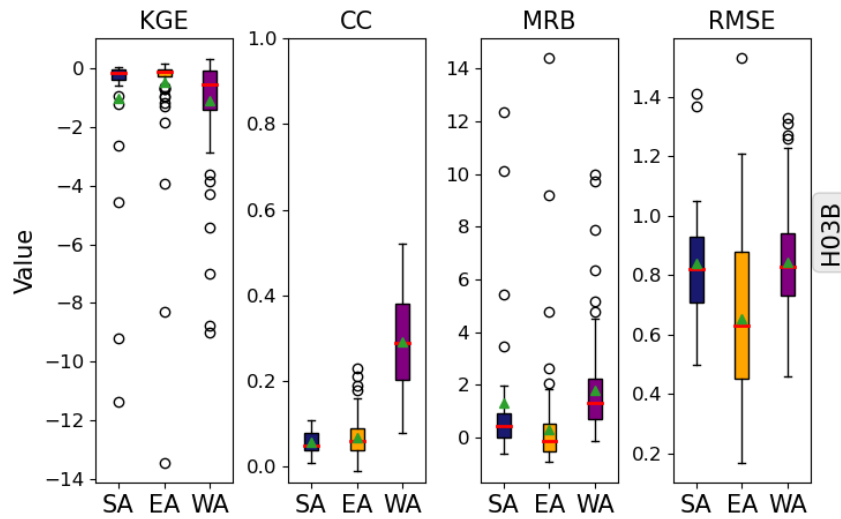

Figure 3 As in Figure 2, but based on quantitative metrics.

Table 3 Evaluation metrics comparing 30-minute satellite and station precipitation estimates

Area	POD	FAR	CSI	Bias	KGE	CC	MRB	RMSE (mm/30min)
SA	0.19	0.90	0.07	1.91	-0.14	0.06	0.48	0.83
EA	0.18	0.88	0.08	1.54	-0.01	0.06	0.05	0.68
WA	0.53	0.81	0.17	2.77	-0.49	0.28	1.20	0.87

Figure 4 and 5 evaluate the satellite products at an hourly time scale analogous to Figure 2 and 3, showing a distribution of 1-hourly metric scores comparable to the 30-minute scores. Table 4 is analogous to Table 3. Figure 6's scatter plot comparison is based on the mixed space-time dataset that computed the metrics in Table 4. Together, they provide an average performance of the H03B products per study location.

According to the POD and CSI scores, detection remains better in WA compared to SA and EA (Figure 4). On average, Table 4 shows only a marginal improvement in detection performance compared to the 30-minute evaluation scores. Per quantitative estimation skill, CC and KGE are only marginally better than 30-minute estimates, whereas estimation bias and error dynamics are similar to the 30-minute evaluation time scale.

Table 4 As in Table 3, but for a 1-hour evaluation time scale

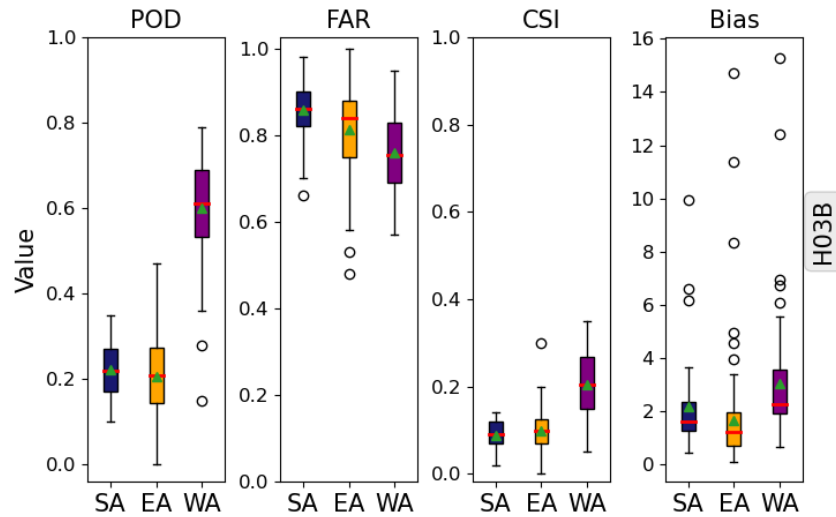| Area	POD	FAR	CSI	Bias	KGE	CC	MRB	RMSE (mm/30min)
SA	0.22	0.87	0.09	1.67	-0.11	0.06	0.48	1.48
EA	0.21	0.85	0.10	1.38	0.02	0.07	0.05	1.17
WA	0.57	0.77	0.20	2.49	-0.46	0.31	1.20	1.54

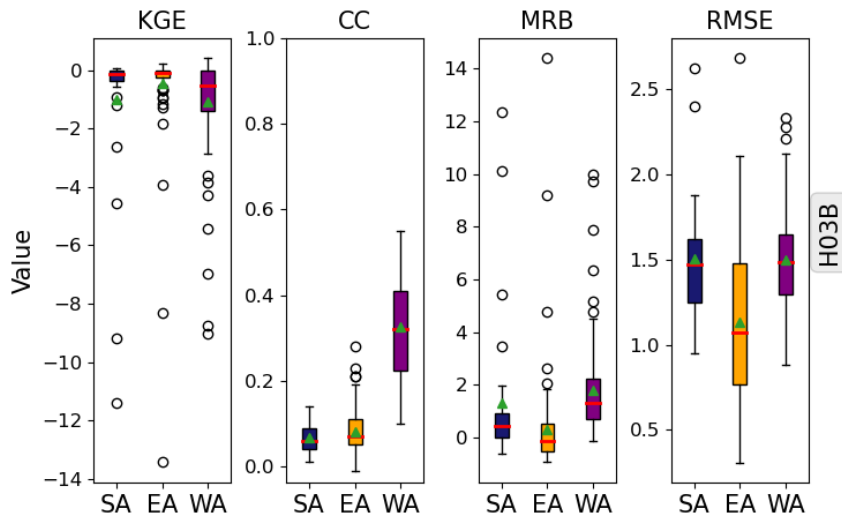Figure 4 As in Figure 2, but for hourly evaluation time scale

Figure 5 As in Figure 3, but based on the hourly evaluation time scale
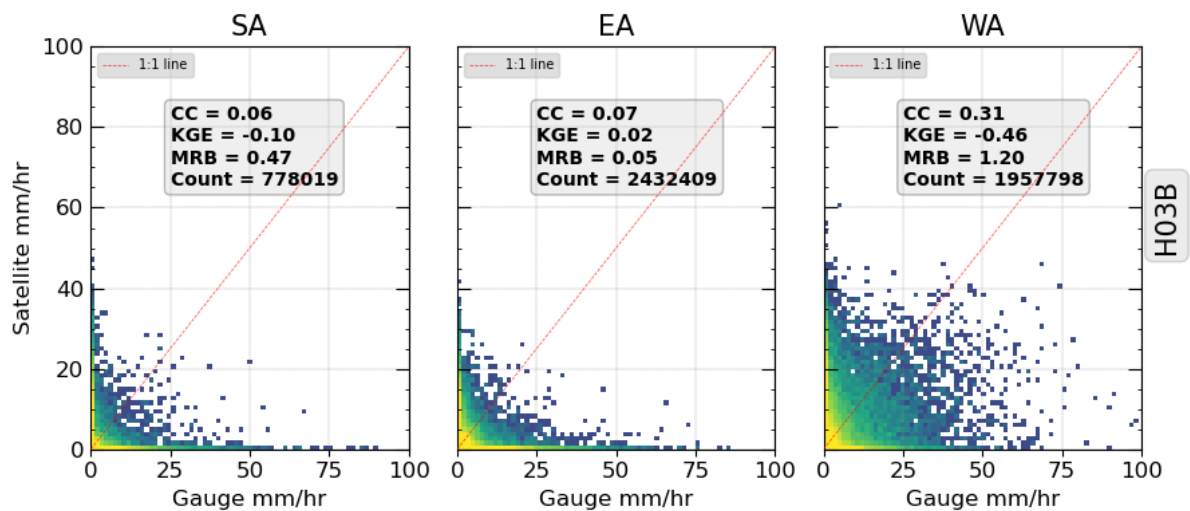

Figure 6 Scatter plot comparison of 1-hourly satellite and gauge precipitation estimates.

H03B's capability of capturing the mean precipitation at each hour of the day, relative to the gauge data, was also investigated using randomly selected gauges, see Figure 7. The focus was on each location's precipitation seasons to account for seasonal variations. The investigation in SA used precipitation data from Malawi, where the rainfall season occurs between November and March. Here, the satellite shows a tendency to overestimate early morning hours precipitation. It misses mid-day precipitation, whereas late afternoon hours are well captured.

EA's investigation used data from Kenya, where a bimodal precipitation season occurs, first between March and June and next between October and December. During the March to June season, H03B captures morning hours precipitation dynamics quite well but overestimates late afternoon precipitation. It missed towards-mid-day precipitation for the October – December season and captured those at every other hour. In WA, it overestimated the mean precipitation at each hour, except the hours between late morning and midday.
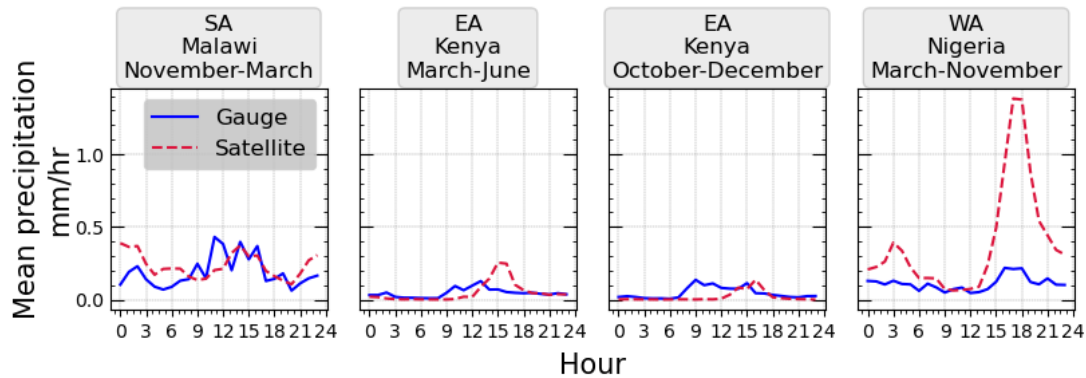
Figure 7 Comparing the satellite and gauge's mean precipitation at each hour of the day.
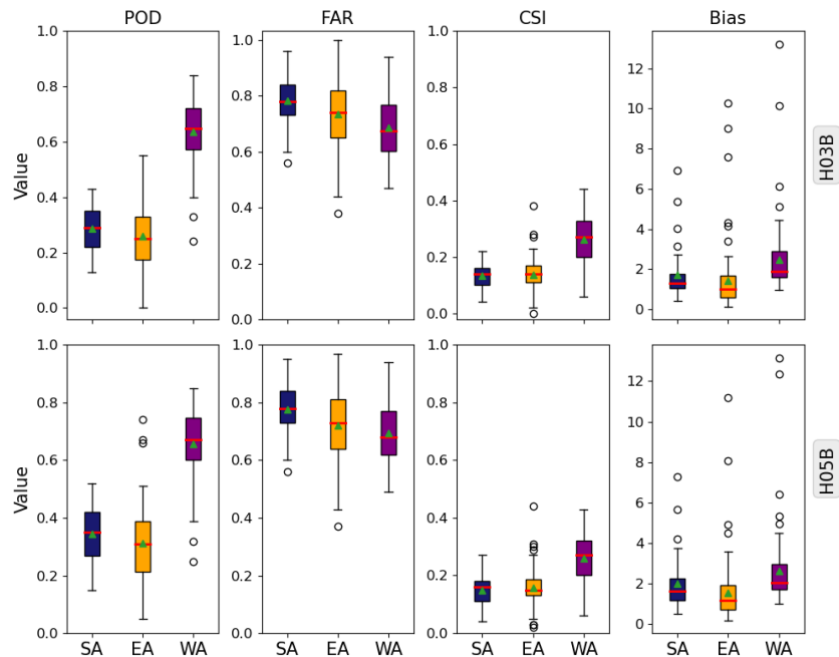
Figure 8 As in Figure 2, but for 3 hourly evaluation time scale

Like Figure 2 and 3, Figure 8 and 9 show the distribution of categorical and quantitative metrics comparing H03B and H05B to the gauge's estimate at each location's station pixel at 3 hourly time evaluation time scales. Figure 10 and Table 5 use mixed space-time observation per each study location to construct a scatterplot and compute its metrics, presenting the average H03B and H05B performance at a 3-hour evaluation time scale similar to the previous 30-minute and 1-hour results.

Notably, both products demonstrate comparable detection performance (Figure 8 and Table 5), which is unsurprising, considering the H05B is derived by temporally integrating the H03B product to 3 hourly intervals. Both products also have better detection performance in WA than in SA and EA based on the POD and CSI values. Their FAR and Bias remain high and comparable to previous 30-minute and 1-hourly evaluation results, and their low CSI point toward weak detection skills (Figure 8, Table 5).

Concerning quantitative estimation, the MRB shows all products have a wet bias, which can be inferred from Figure 10. However, this is lower in EA and SA than in WA, which is attributed to WA's high detection bias (see Table 5). CC, however, shows a better agreement between the gauge and satellite data in WA than SA and EA, which may be attributed to better detection in WA. Average errors are often above 2 mm/3-hours, and KGE, except in EA, is below 0 (Table 5).
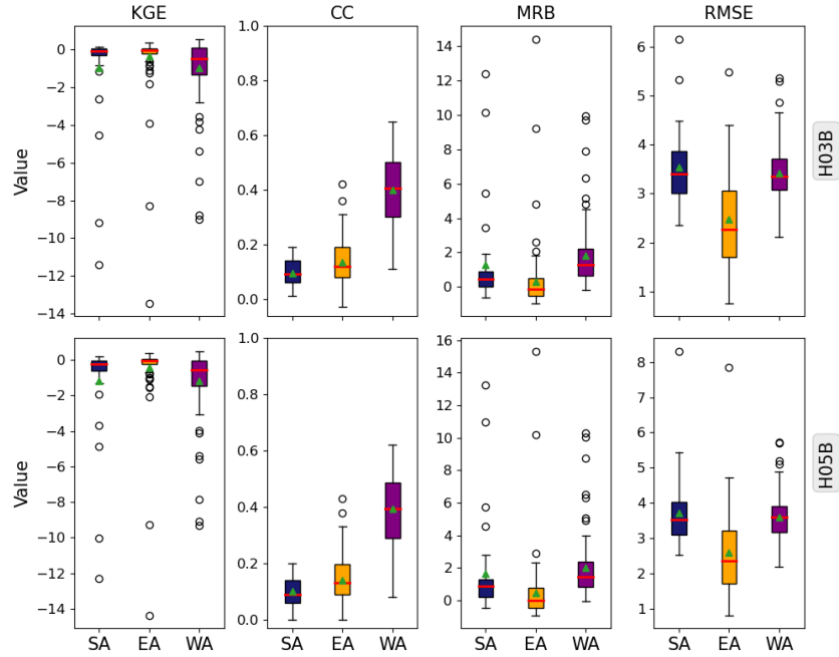
Figure 9 As in Figure 3, but based on 3 hourly evaluation time scales.

Table 5 As in Table 3, but for a 3-hour evaluation time scale

Metric	SA		EA		WA	
	H03B	H05B	H03B	H05B	H03B	H05B
POD	0.28	0.33	0.27	0.31	0.62	0.64
FAR	0.80	0.79	0.77	0.76	0.70	0.71
CSI	0.13	0.15	0.14	0.16	0.25	0.25
Bias	1.38	1.58	1.17	1.32	2.06	2.18
KGE	-0.05	-0.19	0.10	0.08	-0.39	-0.53
CC	0.09	0.10	0.12	0.12	0.38	0.37
MRB	0.48	0.72	0.05	0.19	1.20	1.35
RMSE (mm/3-hrs)	3.47	3.60	2.55	2.65	3.51	3.70
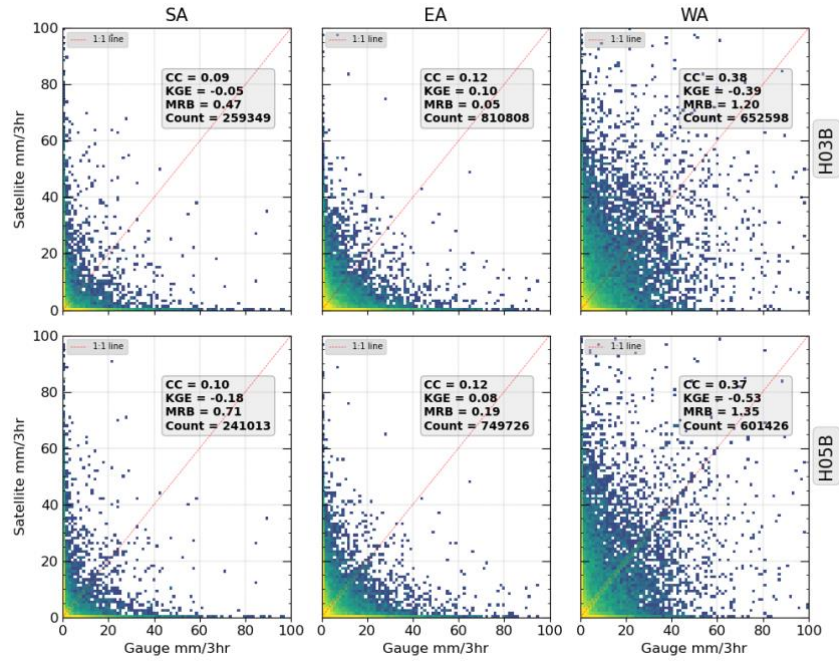
Figure 10 As in Figure 6, but for 3 hourly evaluation time scale

4.1.1.2 The daily evaluation

At the daily scale, all products, H03B, H05B, H64, and H68, were available with sufficient data count, allowing for an evaluation of the products by their Cumulative Distribution Function (CDF) relative to the gauge estimates (Figure 11), and intercomparing their performance across products and locations.
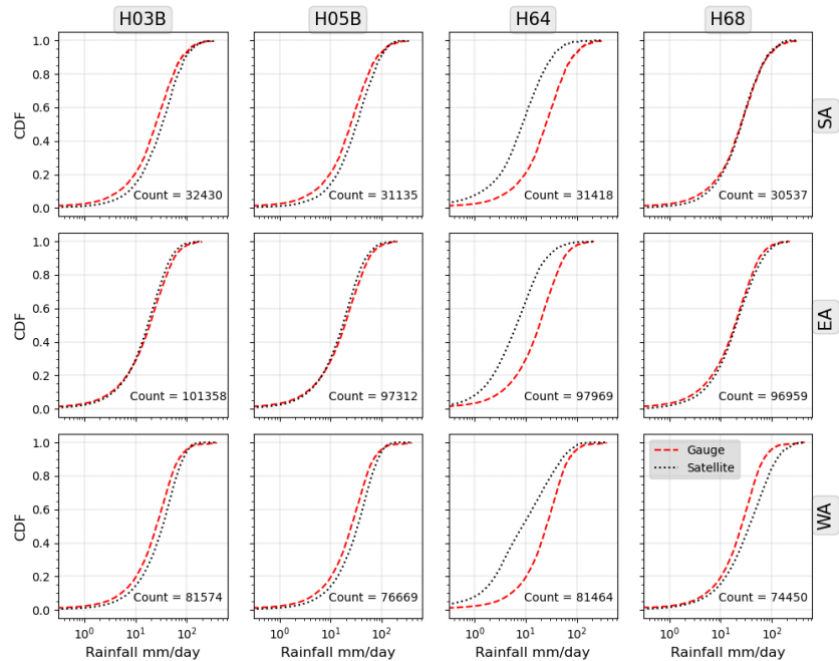
Figure 11 Comparing the CDF of gauge and satellite estimates across locations and products. The number in the plot indicates the sample size that estimated the CDF.

The plot reveals comparable H03B and H05B estimates that reasonably match the gauge estimates, especially in EA, as was observed in previous performance during the sub-daily evaluation. H64 underestimates daily precipitation relative to the gauge, regardless of the location. The H68 product matches the gauge CDF well in SA and EA but overestimates WA's high daily precipitation estimates.
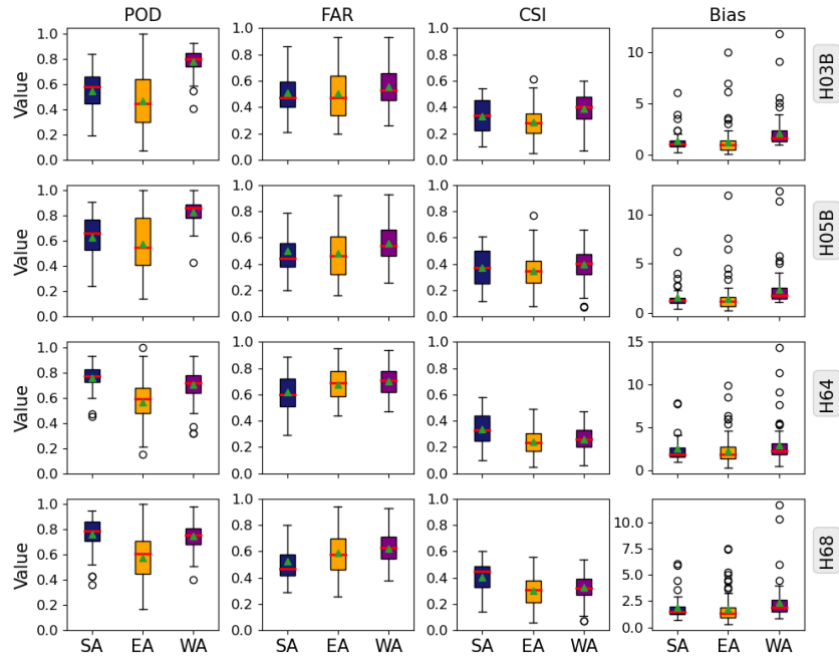
Figure 12 As in Figure 2, but for a daily evaluation time scale

All products' detection and estimation capability is presented in Figures 12, 13, 14, and Table 6, analogous to the previous sub-daily scale analysis. The detection performance of H03B and H05B (in Figure 12 and Table 6) improved compared to their sub-daily evaluation results based on their POD and CSI scores. Additionally, all products show better detection skills in SA and WA than in EA, according to Figure 12 and Table 6. Their average CSI and Bias (Table 6) show the superior performance of the H03B and H05B products compared to H64 and H68 at all locations. Nonetheless, FAR was reasonably higher, often above 0.5, at all locations and by all products (Table 6).
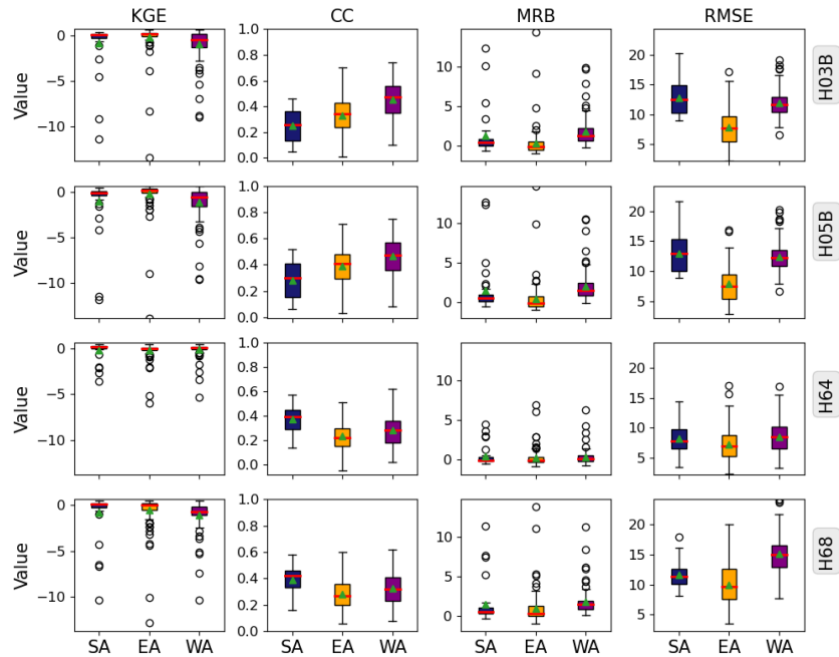
Figure 13 As in Figure 3, but for a daily evaluation time scale

Regarding their quantitative precipitation estimation skill, the H03B and H05B products demonstrate superior performance in EA, according to Figure 13 and Table 6's KGE and CC values. Though their CC was equally high in WA, the KGE values showed weak performance. Overall, they also show an improvement in quantitative estimation skills compared to their previous sub-daily results.

Table 6 As in Table 3, but for a daily evaluation time scale

| Metric	SA				EA				WA			
	H03B	H05B	H64	H68	H03B	H05B	H64	H68	H03B	H05B	H64	H68
POD	0.54	0.62	0.76	0.75	0.49	0.60	0.59	0.59	0.77	0.82	0.71	0.73
FAR	0.54	0.52	0.65	0.53	0.55	0.52	0.69	0.61	0.57	0.57	0.72	0.63
CSI	0.33	0.37	0.31	0.40	0.31	0.36	0.25	0.31	0.38	0.39	0.25	0.32
Bias	1.16	1.30	2.19	1.60	1.08	1.24	1.94	1.50	1.78	1.92	2.52	1.98
KGE	0.10	-0.01	0.22	0.04	0.31	0.33	0.13	0.05	-0.36	-0.53	0.17	-0.52
CC	0.24	0.27	0.35	0.38	0.32	0.38	0.21	0.28	0.42	0.44	0.24	0.30
MRB	0.48	0.68	0.05	0.69	0.05	0.19	-0.03	0.59	1.20	1.39	0.09	1.33
RMSE (mm/day)	12.59	12.85	8.38	11.53	8.06	8.03	7.41	10.13	12.23	12.76	9.08	15.70

H64 was superior in SA and WA, whereas H68's best performance was in SA. The MRB shows that all products often had wet bias at all locations, albeit lowest in EA. Also, H64 had the lowest MRB at all locations, which may be because it underestimated the gauge's CDF in Figure 11. Moreover, the average errors by all products were lowest in EA compared to SA and WA, and H64 had the least errors. Also, H64's KGE is consistently positive in all locations, indicating its robust estimation skill. The H68 product outperformed H03B and H05B products based on the KGE and CC values. However, its performance in EA and WA was weak compared to all other products.
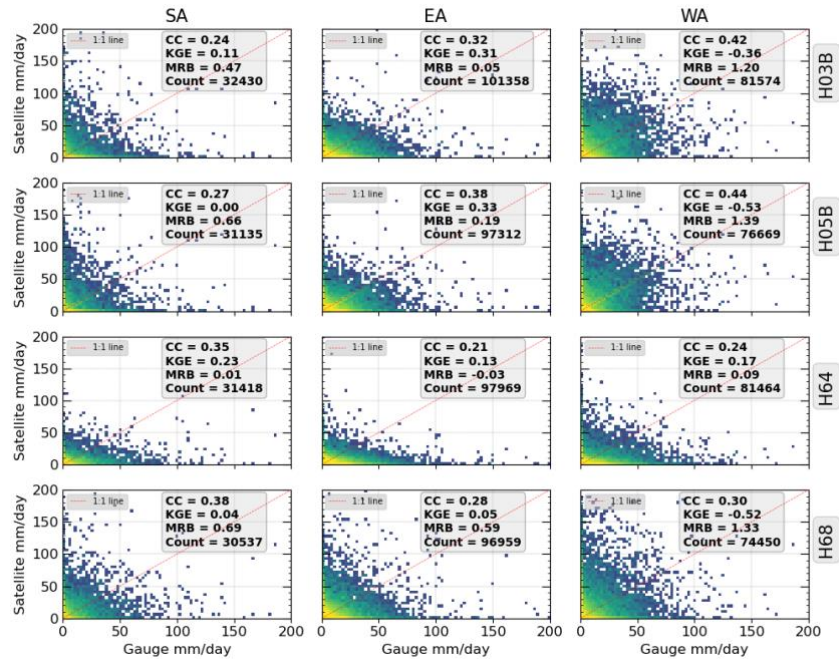
Figure 14 As in Figure 6, but for a daily evaluation time scale

Figure 15 evaluated each product's ability to capture the dynamics of the mean precipitation on each day of the month per each location's precipitation season. The H03B and H05B products demonstrated superior performance in EA for all seasons, corroborating Table 6's results. H64 and H68 products captured the mean precipitation for October – December but overestimated the estimates for March–June.

The H03B, H05B, and H68 often overestimated the mean precipitation in SA and WA, whereas H64 underestimated the mean precipitation in SA but was superiorly in WA, in line with their average errors and biases, both being highest in this location (Table 6).
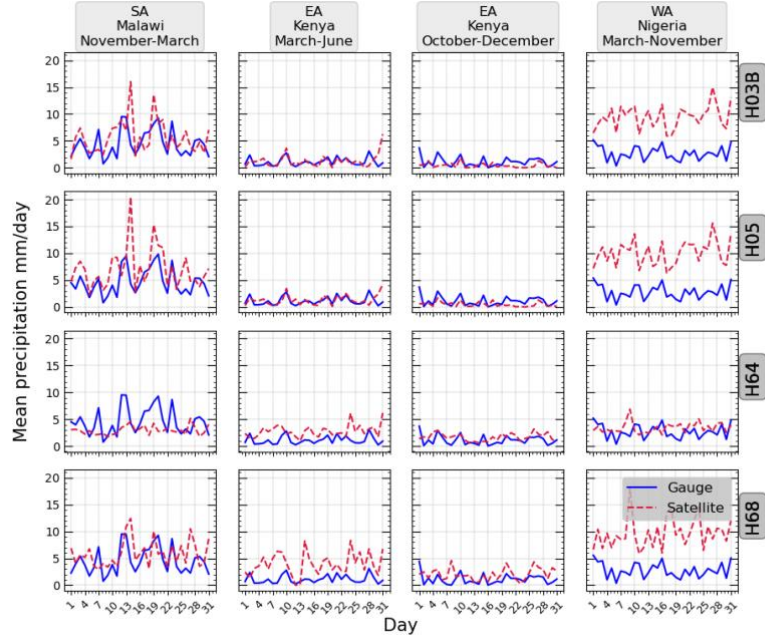
Figure 15 As in Figure 7, but for a daily evaluation time scale.

4.1.2.3 The dekadal evaluation

Figure 16 and 17 present the categorical and quantitative metrics analogous to Figure 2 and 3, while Figure 18 and Table 7 serve the same purpose as Figure 6 and Table 3, respectively. The results show that at the dekadal time scale, the detection performance of all products improved significantly compared to their daily and sub-daily time scale evaluations. Their POD and CSI averages are above 0.8 and 0.5, respectively, in Figure 16 and Table 7, whereas FAR remained below 0.5. H03B and H05B had the lowest detection bias in all locations compared to H68 and H68 products.
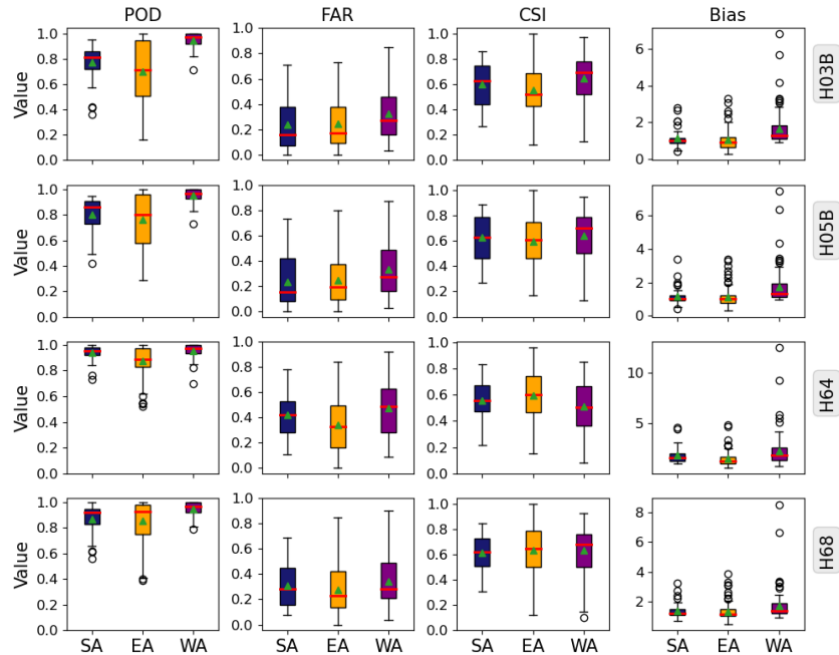
Figure 16 As in Figure 2, but for a dekadal evaluation time scale.
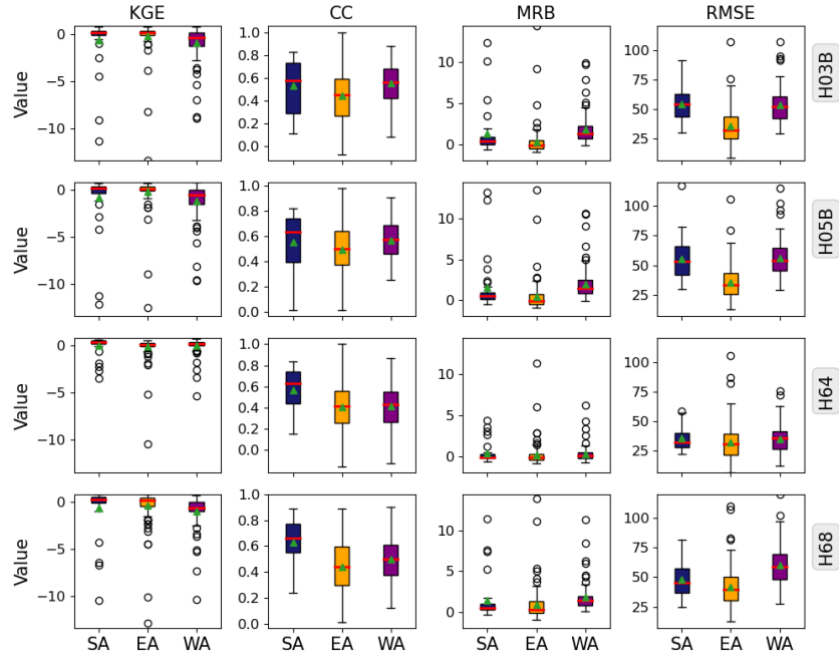
Figure 17 As in Figure 3, but for a dekadal evaluation time scale.

The KGE and CC show that all products performed better in SA and EA than in WA (Figure 17 and Table 7). Compared to the other products, H64 demonstrated superior performance in WA. Also, the average CC values in Table 7 by all products indicate an improvement in their agreement with the gauge estimates compared to their daily and sub-daily results. Moreover, biases, though often wet, especially in WA (Figure 18), are lowest in H64 compared to the other products. Average errors are noticeably high compared to previous daily and sub-daily results.

Table 7 As in Table 3, but for a dekadal evaluation time scale.

| Metric	SA				EA				WA			
	H03B	H05B	H64	H68	H03B	H05B	H64	H68	H03B	H05B	H64	H68
POD	0.74	0.78	0.93	0.85	0.71	0.78	0.89	0.87	0.94	0.95	0.95	0.94
FAR	0.26	0.26	0.45	0.31	0.26	0.26	0.35	0.29	0.33	0.34	0.47	0.34
CSI	0.59	0.61	0.53	0.61	0.57	0.61	0.60	0.64	0.64	0.64	0.51	0.63
Bias	1.01	1.04	1.69	1.22	0.97	1.05	1.36	1.21	1.41	1.44	1.81	1.43
KGE	0.31	0.16	0.42	0.18	0.43	0.44	0.27	0.18	-0.33	-0.50	0.29	-0.46
CC	0.51	0.52	0.53	0.61	0.44	0.48	0.33	0.46	0.50	0.51	0.37	0.45
MRB	0.48	0.68	0.03	0.69	0.05	0.19	-0.04	0.59	1.20	1.39	0.09	1.33
RMSE (mm/month)	54.35	56.81	36.48	49.02	37.58	37.40	33.69	44.07	56.48	58.96	37.90	63.72
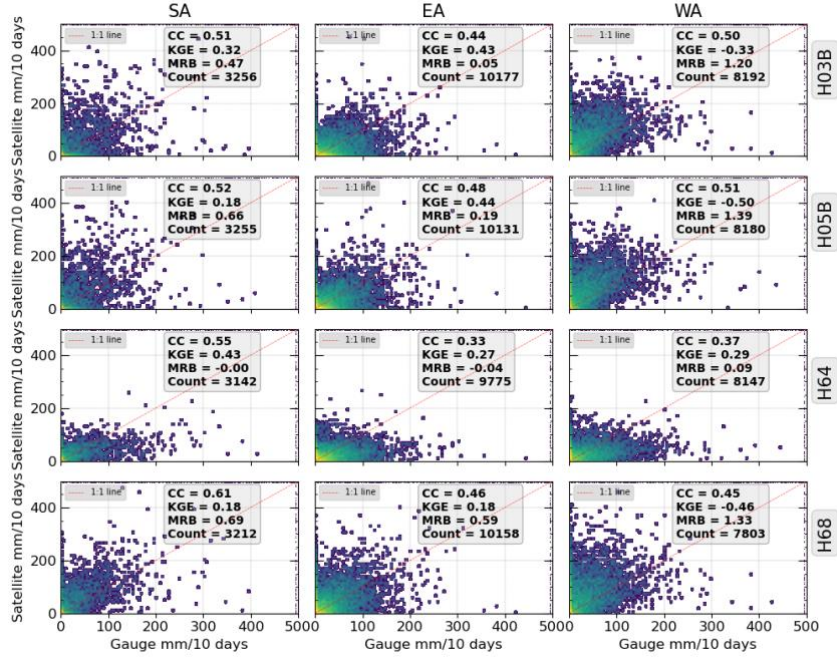
Figure 18 As in Figure 6, but for a dekadal evaluation time scale.

4.1.2.4 The monthly evaluation

Figure 19 presents the distribution of categorical metrics computed during the monthly evaluation scale at each location's station pixel, similar to Figure 2. Table 8 provides an average detection performance from a mixed space-time dataset perspective. Clearly, each product's detection skill improved significantly, indicated by the high POD and CSI coupled with low FAR scores compared to its daily and sub-daily metrics. Nonetheless, detection bias remains higher in WA compared to SA and EA.

Figure 19 As in Figure 2, but for a monthly evaluation time scale.
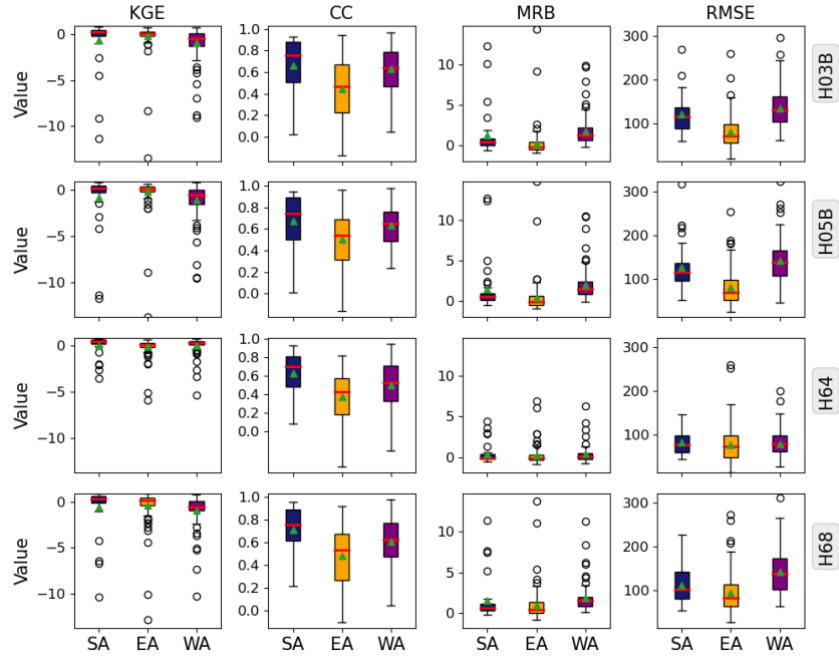
Figure 20 As in Figure 3, but for a monthly evaluation time scale.

Per their quantitative metrics (Figure 20 and Table 8), KGE and CC indicate better performance in SA and EA than in WA, corroborating previous dekadal results. More specifically, H64 demonstrates superior performance in SA and WA based on its KGE and MRB values, whereas the H03B and H05B products had their best performance in EA. For the H68 product its performance was often weak compared to the other products, according to its KGE. Additionally, Table 8 and Figure 21 indicate that wet bias and average errors are highest in WA compared to SA and EA, although the H64 had the least biases and errors.

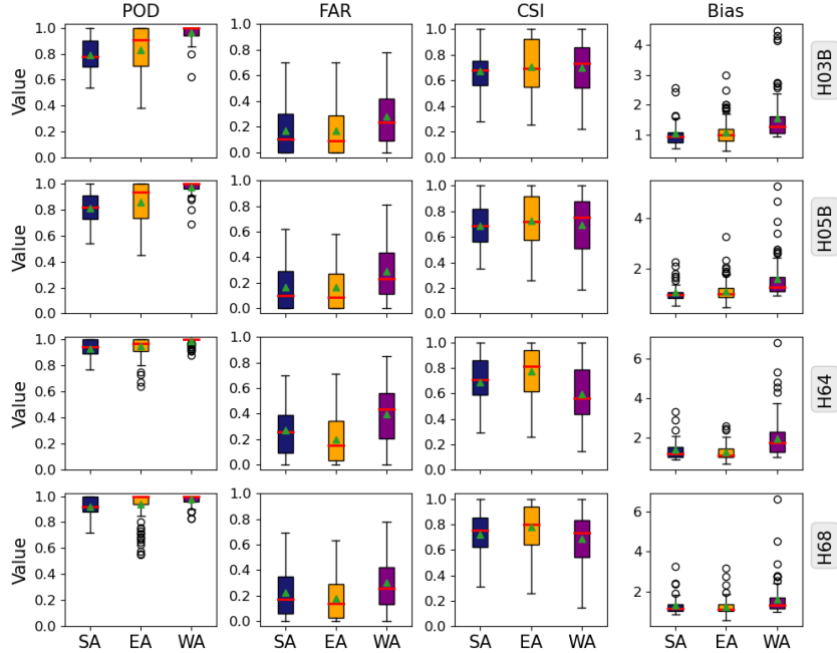
Figure 21 As in Figure 6, but for a monthly evaluation time scale.

Table 8 As in Table 3, but for a monthly evaluation time scale.
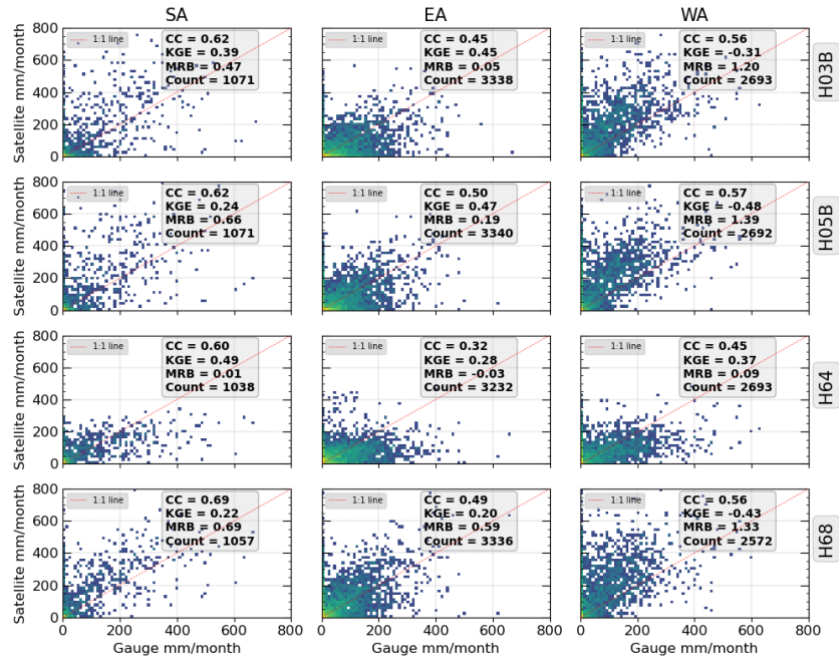
Metric	SA				EA				WA			
	H03B	H05B	H64	H68	H03B	H05B	H64	H68	H03B	H05B	H64	H68
POD	0.78	0.81	0.93	0.92	0.83	0.87	0.95	0.94	0.96	0.98	0.99	0.97
FAR	0.20	0.20	0.30	0.23	0.18	0.18	0.21	0.19	0.29	0.30	0.39	0.30
CSI	0.66	0.67	0.66	0.72	0.70	0.73	0.75	0.77	0.69	0.69	0.60	0.69
Bias	0.97	1.01	1.32	1.19	1.02	1.06	1.20	1.16	1.36	1.39	1.63	1.39
KGE	0.38	0.22	0.47	0.22	0.45	0.47	0.28	0.20	-0.31	-0.48	0.37	-0.43
CC	0.62	0.62	0.59	0.69	0.45	0.50	0.32	0.49	0.56	0.57	0.45	0.56
MRB	0.48	0.68	0.05	0.69	0.05	0.19	-0.03	0.59	1.20	1.39	0.09	1.33
RMSE mm/month	124.21	133.88	85.90	117.64	88.21	88.30	81.80	104.40	144.68	152.38	87.80	153.71

The mean precipitation at each month of the year by the satellite and the gauge is also compared in Figure 22, capturing the precipitation cycle in a year. The figure shows a normalized y-axis to compare results across products and locations. Generally, all products demonstrate capabilities of observing the precipitation cycle in a year, albeit with a slight difference in their estimates compared to the gauge. More specifically, SA's H03B and H05B estimates agree well with the gauge estimate. In contrast, especially for the H64, precipitation is overestimated in the first quarter of the year.

In EA, H03B and H05B agree well with the gauge estimates during the first quarter but underestimated the last quarter of the year estimates. The H64 and H68 products overestimated the mean precipitation from March to May, whereas towards the end of the year, their estimates compared better to the gauge's estimate. At the beginning of the year in WA, all products overestimated precipitation relative to the gauge's estimate. By contrast, they underestimated the mean precipitation from May to August and overestimated the September-October mean precipitation relative to the gauge.
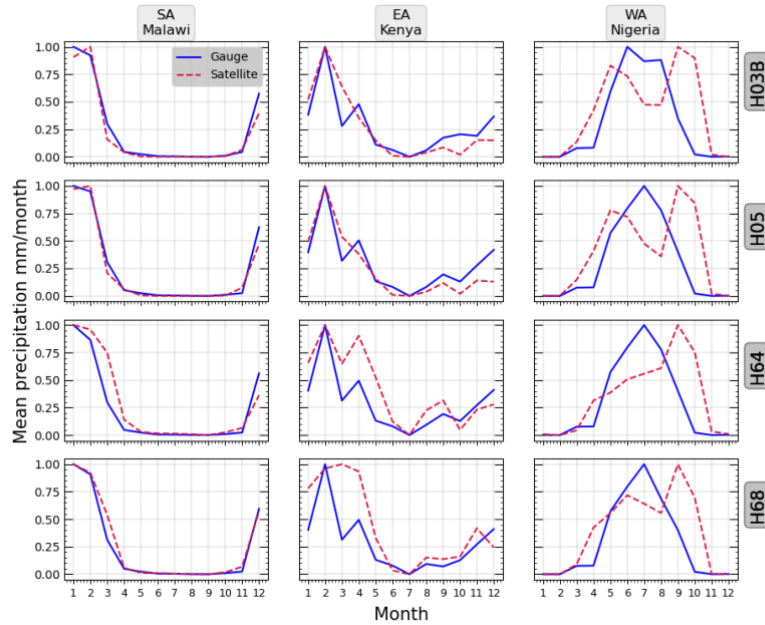

Figure 22 As in Figure 7, but for a monthly evaluation time scale

4.1.2 Capability of H SAF to detect and estimate extreme precipitation

This section presents the H SAF products' extreme precipitation detection and estimation capabilities investigated using 3 different extreme indexes, Ext_{50}, $Ext_{95\%}$, and $Ext_{99\%}$: first, to explore the satellite's detectable range of extreme values and second, to assess the agreement between it and the gauge's extreme precipitation estimates.

Figure 233, 24, and 25 compare the distribution of precipitation extremes by the gauge and satellite according to the Ext_{50}, $Ext_{95\%}$ and $Ext_{99\%}$ extreme indexes to investigate the range of detectable extreme rainfall by the H SAF products. At Ext_{50} (Figure 23), all products detect and estimate a comparable range of extreme precipitation in EA and SA. The H03B, H05B, and H64 have a comparable range of extreme values in WA. Also, the distribution of precipitation extremes below 100 mm/day for all products matches the gauge's distribution quite well. Furthermore, they demonstrate the capability of detecting and estimating precipitation greater than 200 mm/day, particularly in WA. Notably, EA and SA seem to have a lot of extreme precipitation compared to WA, which both the gauge and the satellite agree.
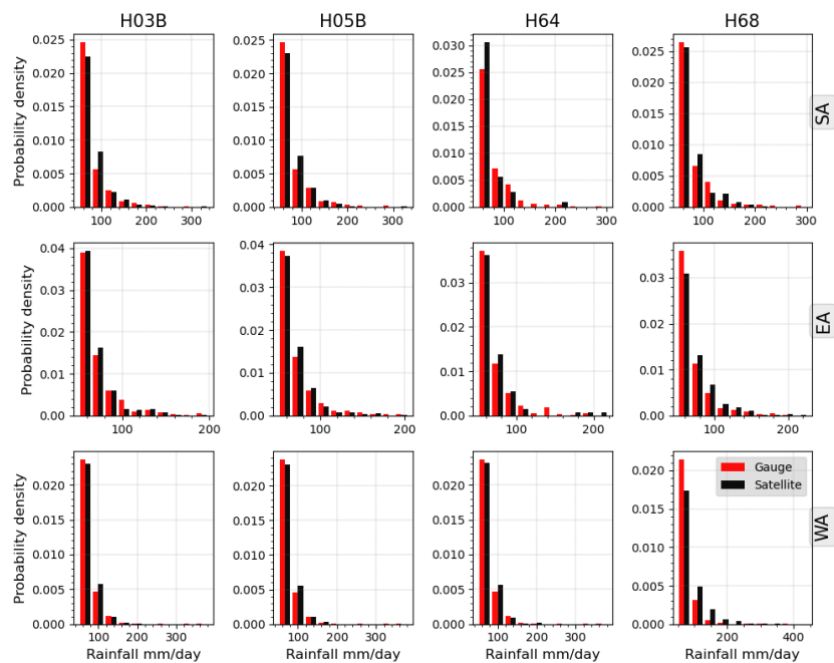
Figure 23 Comparing the distributions of all extreme precipitation by H SAF and the gauge at Ext_{50}.

At $Ext_{95\%}$, the distribution of precipitation extremes by all products reasonably matches the gauge's distribution, with most of it occurring below 100 mm/day. The above 100 mm/day precipitation only constitutes a few samples in the distribution (Figure 24). As in Figure 23, there is also a comparable range of extreme values in SA and EA by all products. In SA, up to 300 mm/day of precipitation was estimated, whereas EA's extreme precipitation was up to 200 mm/day. In some cases, the WA extremes were above 300 mm/day, particularly based on the H68 product.
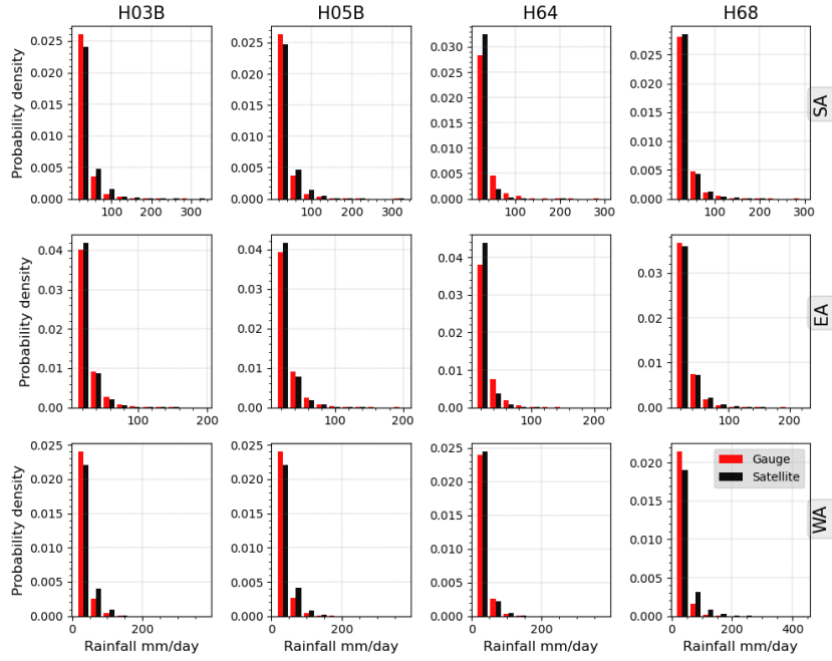
Figure 24 As in Figure 23, but based on $Ext_{95\%}$ extreme index.

As was also observed in Figure 24, the distribution of extreme precipitation values based on $Ext_{99\%}$ (Figure 25) matches the gauge's distribution and are often below 100 mm/day. The range of extreme precipitation values per location and product is also similar to the previous $Ext_{95\%}$ results.
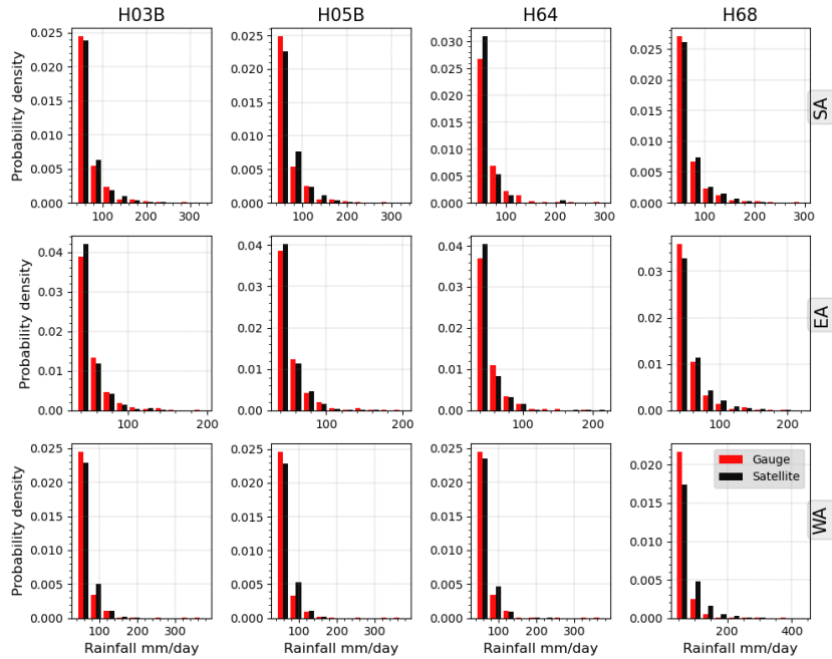
Figure 25 As in Figure 23 but based on $Ext_{99\%}$ extreme index

Figure 26, 27, and 28 were used to investigate the agreement between the satellite and the gauge's extreme values through the question: when the gauge observed an extreme value, what was the satellite estimate? For these plots, a mixed space-time dataset was constructed using the coincident satellite and gauge precipitation estimate observed at each study location's station pixel. Then, all rows in the dataset where the gauge's estimate is greater than an extreme index were selected to construct each plot's distribution and compute its evaluation metric.
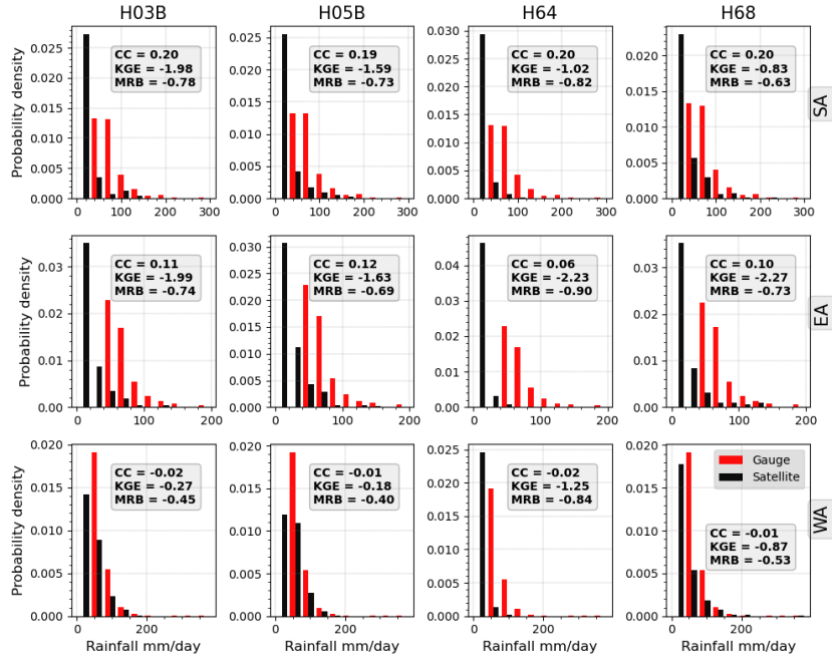
Figure 26 Comparing the distribution of precipitation values of H SAF to the gauge when the gauge detected and estimated an $Ext_{50\%}$ precipitation.

Figure 26 shows that when the gauge detects and estimates a $Ext_{50\%}$ extreme precipitation, the satellite estimate often does not agree with this observation. The satellite's peak distribution below 50 mm/day indicates that when the gauge's daily precipitation exceeds 50 mm, the satellite's estimate is often less than this value. This manifests in KGE values that are often highly negative, close to zero CC values, and significant underestimation (based on MRB values) relative to the gauge's estimate at all locations.
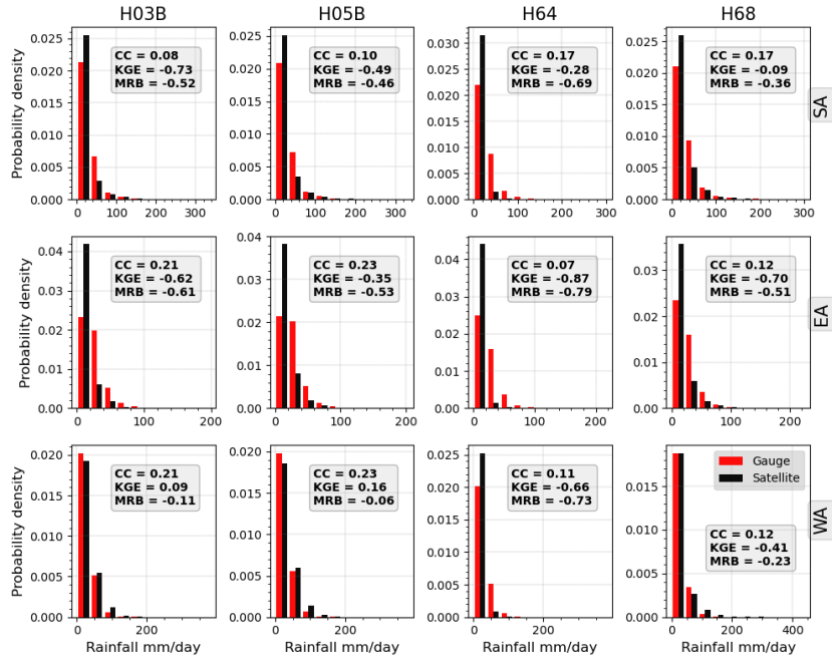
Figure 27 As in Figure 26 but based on $Ext_{95\%}$ index.

Figure 27 is analogous to Figure 26 except based on $Ext_{95\%}$ index criteria. Notably, there is a better match between the gauge and satellite's distribution, particularly in SA and WA, compared to the previous estimates based on $Ext_{50\%}$. Furthermore, H03B, H05B and H68 estimates matches the gauge's distribution quite well for values below 50 mm/day. Location-wise, KGE and MRB indicate H68's superior performance in SA, whereas H03B and H05B are superior in WA. H64 demonstrated the weakest performance. Nonetheless, low CC values indicate that the agreement between the satellite and the gauge is weak overall.

Figure 28 As in Figure 26, but based on $Ext_{99\%}$ extreme index
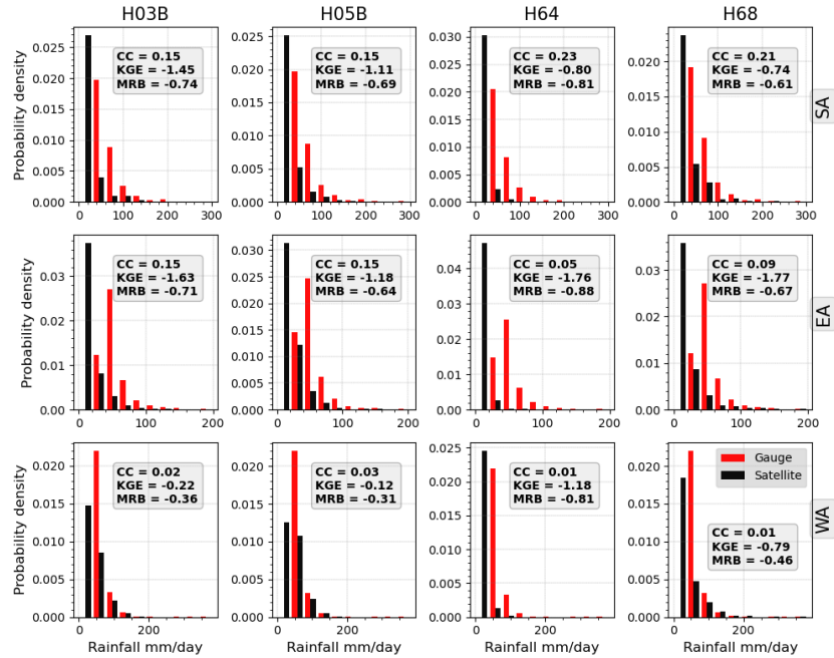
Like in Figure 27, Figure 28 compares the satellite's estimates when the gauge's estimated daily precipitation exceeds the 99th percentile value. Generally, all products underestimate extreme precipitation relative to the gauge at all locations, according to their MRB values. Also, when considering the satellite's peak distribution relative to the gauge's estimate, the satellite's characteristic underestimation becomes even more evident. Besides, low KGE and CC values further magnify the satellite's weak extreme precipitation skill at $Ext_{99\%}$.

However, regardless of the extreme index used in Figure 26, 27, and 28, it is evident that all the products can detect and estimate extreme precipitation values that are sometimes close to 200 mm/day, a characteristic that was also observed when investigating their detectable extreme value ranges in Figure 23, 24, and 25.

4.2 Discussion

This AS activity evaluated H SAF's H03B, H05B, H64, and H68 precipitation products' capability for (a) accurate rainfall detection and estimation at varying temporal scales and (b) detecting and estimating extreme precipitation relative gauge estimate. The latter utilized 3 indices, $Ext_{50\%}, Ext_{95\%}$ and $Ext_{95\%}$, which represents daily precipitation exceeding 50 mm/day, and the 95th and 99th percentiles of rainy days, respectively, to define extreme precipitation.

4.2.1 On the H SAF's precipitation detection performance at varying temporal scales

   I.   The sub-daily temporal evaluation scale performance

At the sub-daily temporal scale, the H03B and H05B products were evaluated at 30-minute, 1-hourly (mainly for the H03B), and 3-hourly (H03B, H05B) evaluation time scales. The results indicate better detection in WA than in SA and EA, with a POD value of 0.5 on a 30-minute and 1-hourly evaluation

time scale and 0.6 for a 3-hourly time scale. Nevertheless, all products' overall FAR and detection bias were high, and their CSI was low, suggesting a weak sub-daily precipitation detection skill.

II.   The daily to monthly evaluation scale performance

All products were evaluated at the daily – monthly evaluation time scale. On a daily scale, the H03B and H05B products saw improved performance relative to their sub-daily performance. Additionally, all products detect precipitation better in SA and WA than in EA. More specifically, in all locations, CSI and detection bias by H03B and H05B were higher and lower, respectively, than those of H64 and H68. Regardless, all products' FAR were noticeably high in all locations.

Results at the dekadal and monthly scales show significant improvement in precipitation detection performance by all products compared to sub-daily and daily evaluation time scales, indicated by high POD (> 0.8) and CSI (approximately 0.5), with low FAR (often below 0.4) in all locations. However, the products tend to over-detect dekadal and monthly scale precipitation in WA compared to SA and EA.

The weak sub-daily detection performance observed, particularly in EA and SA, may be attributed to factors such as the complex local and large-scale phenomena that affect EA and SA precipitation [12]. For instance, DEM in Figure 1 shows that the topography in SA and EA is much more complex than in WA, which challenges accurate satellite precipitation observation in these areas [2, 20]. Also, H03B and H05B's retrieval algorithm focuses on cold cloud tops in GEO IR observations and may miss precipitation in relatively warm clouds generated through the orographic precipitation process, which may explain their low POD scores in SA and EA. By contrast, H64 and H68 are microwave-based products relying on MW brightness temperatures more related to precipitation hydrometeors, resulting in relatively good POD scores. However, the MW signals' oversensitivity to low precipitation [21] may explain their high detection bias compared to the H03B and H05B products in all locations.

4.2.2 On the H SAF precipitation estimation performance

I.   The sub-daily quantitative precipitation estimation performance

The sub-hourly to hourly CC values indicate weak agreement between the H03B and gauge estimates. Location-wise, the results show better agreement in WA than in SA and EA. MRB suggests wet bias, but this tends to be lower in SA and EA than in WA. The average errors (RMSE) between H03B and the gauge are comparable in SA and WA and lower in EA. Overall, KGE suggests a weak sub-daily precipitation estimation skill by H03B, irrespective of location.

The capability of the H03B product to estimate the mean precipitation at each hour of the day relative to the gauge was also investigated using randomly selected gauges that had sufficient observations during the evaluation period. The focus was on each location's precipitation season to account for variations in hourly precipitation. In SA, the investigation used data from Malawi, where the precipitation season occurs between November and March. H03B overestimated precipitation during early morning hours. It missed the mid-day precipitation, whereas, for late afternoon hours, it captured the precipitation quite well.

EA's investigation used Kenya data, which has a bimodal precipitation season, first occurring between March and June and next between October and December. H03B captured morning hours precipitation dynamics quite well during the March to June season but overestimated late afternoon precipitation. It missed the precipitation occurring towards mid-day during the October – December season and captured those at every other hour. For WA, it overestimated the mean precipitation at each hour, except the hours between late morning and midday.

II.   The performance at the daily – monthly evaluation time scale

First, the CDF of all products was compared to the gauge's CDF at the daily scale, revealing that the H64 product tends to underestimate the daily precipitation relative to the gauge. H03B and H05B estimates match the gauge's estimate in EA. H68's estimates match the gauge quite well in SA and EA but overestimated WA's high daily precipitation estimates.

The CC values indicate that the agreement between the H03B and H05B and the gauge data only saw marginal improvement relative to their sub-daily performance. Judging by their KGE and CC, they also estimate precipitation better in EA than in SA and WA. H64's KGE was consistently positive in all locations, suggesting robust estimation skills, particularly better in SA and WA. For H68, its best performance was in SA.

Regarding their estimation biases relative to the gauge's estimate, the H64 products had the lowest bias, often less than 10% wet bias, except in EA, where it underestimated the gauge's estimate by 3%. All other products demonstrated wet bias relative to the gauge in all locations, specifically low in EA and highest in WA. Also, the H68 biases were the highest in all locations compared to all other products. Regarding the average errors between the gauge and satellite estimates, all products had minimal errors in EA compared to SA and WA. The H03B and H05B products had maximum errors in SA, whereas for H64 and H68, this was in WA.

The mean precipitation on each day of the month during the evaluation period was also investigated, analogous to the hourly investigation. All products captured the dynamics of the mean precipitation in EA, particularly the October-December seasons, which correlates with the location's low biases observed by the products. In SA and WA, the H03B, H05B, and H68 products often overestimated the mean precipitation, whereas H64 underestimated the mean precipitation in SA but was superior in WA.

At the dekadal and monthly, KGE suggests that all products demonstrate robust estimation skills in SA and EA, where they had positive values. Besides, the average errors and biases were also lowest in these areas. KGE, MRB, and RMSE suggest the products had the worst performance in WA. Overall, their dekadal and monthly quantitative metrics point towards an improved skill relative to their daily and sub-daily metrics.

Similarly, all products' mean precipitation per month of the year was also evaluated relative to the gauge's estimate. Overall, all products captured the yearly precipitation cycle. More precisely, H64 and H68 overestimated SA's beginning-of-the-year precipitation. H03B and H05B slightly underestimated towards the end of the year precipitation in EA, whereas for H64 and H68 products the March-May precipitation was overestimated. For WA, all products overestimated the mean precipitation during the beginning of the year and September to October, while they underestimated the May to August mean precipitation.

Many factors may explain the disparity between the satellite and the gauge estimates. For instance, the fact that this study compares gauge estimates (representing point observation) to satellite pixel estimates may contribute to these differences in precipitation estimates. The gauge's observation technique is such that it accumulates precipitation from a single point, whereas the satellite averages an observation over a pixel. Additionally, high spatial and temporal precipitation variability contributes to these differences in precipitation estimates by the gauge and satellite [2, 22, 23].

Aggregation through daily to monthly temporal scales significantly improved the performance of all products, an observation Macharia, et al. [5] also made when comparing satellite to gauge data over the study area. Nevertheless, disparities exist between the gauge and satellite's mean precipitation, especially at the hourly and monthly scales. This may be improved by adjusting the satellite estimates to each location's mean precipitation climatology, inferred from Global Precipitation Climatology Centre (GPCC) gauge data, as pointed out by Funk, et al. [22].

4.2.3 The extreme rainfall detection and estimation performance of the H SAF products

Three indexes: Ext_{50}, $Ext_{95\%}$, and $Ext_{99\%}$ investigated the H SAF products' daily extreme precipitation detection and estimation capabilities to reveal the satellite's detectable range of extreme values and to assess its agreement with the gauge's estimate. The results show that most of the extreme precipitation detected and estimated by the products is below 100 mm/day, and its distribution matches the gauge's estimate quite well in all locations. In SA and EA, extreme precipitation reached about 300 and 200 mm/day, respectively, whereas WA's extreme precipitation was over 300 mm/day, to which all the products agree.

Regardless, the overall agreement between the gauge and satellite's estimates was weak, suggesting that although the products can capture extreme precipitation values, they may not always agree with the ground observations, limiting their hydro-meteorological applications in, e.g., flood, dam, and water reservoir management.

4.2.4 The Study Implications

The results of this study indicate that the H SAF products demonstrate satisfactory precipitation estimation skills at dekadal to monthly time scales, which is valuable for agriculture and drought monitoring applications that require coarse temporal scale precipitation data. Nevertheless, the high biases and errors found in this study may require bias adjustment of the products using, e.g., statistical techniques that consider the local characteristics of climatological mean before their use in these applications. Concerning their extreme precipitation detection and estimation skills, the products demonstrated capabilities in detecting and estimating over 100 mm/day precipitation – the kind of precipitation accumulations capable of triggering natural disasters like flooding and landslides. Yet, the low agreement with ground observations remains concerning and may require further studies.

5.0 Conclusion

Four H SAF precipitation products, H03B, H05B, H64, and H68, were evaluated using gauge data in Western, Eastern, and Southern Africa during 2020 – 2022, revealing their precipitation estimation skills in a sparsely gauged region. The evaluation focused on 2 primary goals:

1. to assess the products' accuracy at different temporal scales and intercompare their performances in the different SSA regions and,
2. to assess the capability of the different H SAF precipitation products to detect and estimate extreme rainfall in SSA.

Regarding precipitation detection, the results indicate weak H03B and H05B sub-daily detection skills, regardless of location. The daily evaluation scale saw improvement in product detection skills but differed per location. Specifically, H03B and H05B tend to be better in WA, whereas the results for H64 and H68 show a better performance in SA and WA. All products demonstrated their best performance at the dekadal to monthly scale, albeit with a slight over-detection tendency in WA.

Quantitatively, KGE, CC, and MRB results judge H03B and H05B products as having weak sub-daily precipitation estimation skills. At the daily evaluation time scale, H03B and H05B's precipitation estimates agree better with gauge estimates in WA and SA. In contrast, the H64 and H68 products demonstrate better agreement with estimates in SA. Although all the products often had a wet bias in all locations, H64 notably had the lowest bias. Also, H64 had the lowest errors on the daily time scale compared to all other products. All products had minimum and maximum errors in EA and WA, respectively. The precipitation estimation skill of all products was best at the dekadal and monthly time scales according to KGE and CC. Still, their average errors were relatively high compared to daily and sub-daily results.

Concerning extreme precipitation detection and estimation, all products agree with the gauge that most extreme precipitation over the study area is below 100 mm/day. They also captured 200 and 300 mm/day maximum extreme precipitation in SA and EA, respectively, whereas they suggested over 300 mm/day precipitation for WA. However, their overall agreement with the gauge data was weak.

This study acknowledges the sparse distribution of its ground observations, which may limit the generalization of each location's results. Regardless, data from over 200 stations between 2020 and 2022 can capture valuable temporal and spatial precipitation characteristics capable of evaluating the satellite products.

Though there exist apparent disparities between the satellite and ground precipitation that can be attributed to factors including differences in their measurement techniques, these findings may have implications on the H SAF precipitation products' applications, e.g., in agriculture, water resources management, and flood and drought monitoring in these areas where conventional ground rainfall

monitoring systems are scarce or inadequate. Besides, for the rainfall retrieval algorithm developers, these results from largely unmonitored areas provide a new perspective on the performance of rainfall retrieval in these areas, which may inform future satellite rainfall retrieval missions.

6.0 Acknowledgment

7.0 References

[1]   K. K. Kumah, "Near-real-time rainfall detection and estimation from commercial microwave links and Meteosat Second Generation data," PhD, Water Resources, University of Twente, Faculty of Geo-Information Science and Earth Observation (ITC), Enschede, 420, 2022. [Online]. Available: https://dx.doi.org/10.3990/1.9789036554589

[2]   K. K. Kingsley, B. H. P. Maathuis, J. C. B. Hoedjes, D. T. Rwasoka, B. V. Retsios, and B. Z. Su, "Rain Area Detection in South-Western Kenya by Using Multispectral Satellite Data from Meteosat Second Generation," *Sensors (Basel),* vol. 21, no. 10, May 19 2021, doi: 10.3390/s21103547.

[3]   T. Dinku, "Challenges with availability and quality of climate data in Africa," in *Extreme Hydrology and Climate Variability*, 2019, pp. 71-80.

[4]   M. W. Kimani, J. C. B. Hoedjes, and Z. Su, "An assessment of satellite-derived rainfall products relative to ground observations over East Africa," (in English), *Remote Sensing,* vol. 9, no. 5, May 2017, doi: 10.3390/rs9050430.

[5]   D. Macharia, K. Fankhauser, J. S. Selker, J. C. Neff, and E. A. Thomas, "Validation and intercomparison of satellite-based rainfall products over Africa with TAHMO in-situ rainfall observations," *Journal of Hydrometeorology,* 2022, doi: 10.1175/jhm-d-21-0161.1.

[6]   A. K. Dezfuli *et al.*, "Validation of IMERG Precipitation in Africa," (in English), *Journal of Hydrometeorology,* vol. 18, no. 10, pp. 2817-2825, Oct 2017, doi: 10.1175/jhm-d-17-0139.1.

[7]   N. van de Giesen, R. Hut, and J. Selker, "The Trans-African Hydro-Meteorological Observatory (TAHMO)," *Wiley Interdisciplinary Reviews: Water,* vol. 1, no. 4, pp. 341-348, 2014, doi: 10.1002/wat2.1034.

[8]   S. Puca *et al.*, "The validation service of the hydrological SAF geostationary and polar satellite precipitation products," *Natural Hazards and Earth System Sciences,* vol. 14, no. 4, pp. 871-889, 2014, doi: 10.5194/nhess-14-871-2014.

[9]   A. Giannini, R. Saravanan, and P. Chang, "Oceanic forcing of Sahel rainfall on interannual to interdecadal time scales," *Science,* vol. 302, no. 5647, pp. 1027-30, Nov 7 2003, doi: 10.1126/science.1089357.

[10]   B. J. Abiodun, Z. D. Adeyewa, P. G. Oguntunde, A. T. Salami, and V. O. Ajayi, "Modeling the impacts of reforestation on future climate in West Africa," *Theoretical and Applied Climatology,* vol. 110, no. 1-2, pp. 77-96, 2012, doi: 10.1007/s00704-012-0614-1.

[11]   H. S. Endris *et al.*, "Assessment of the Performance of CORDEX Regional Climate Models in Simulating East African Rainfall," (in English), *Journal of Climate,* vol. 26, no. 21, pp. 8453-8475, Nov 2013, doi: 10.1175/JCLI-D-12-00708.1.

[12]   S. E. Nicholson, "Climate and climatic variability of rainfall over eastern Africa," (in English), *Reviews of Geophysics,* vol. 55, no. 3, pp. 590-635, Sep 2017, doi: 10.1002/2016RG000544.

[13] T. J.F *et al.*, "Analysis and Assimilation of Rainfall from Blended SSM/I, TRMM and Geostationary Satellite Data," in *10th Conference on Satellite Meteorology and Oceanography*, 2000, no. 9, pp. 66-69.

[14] Q. Jiang *et al.*, "Evaluation of satellite-based products for extreme rainfall estimations in the eastern coastal areas of China," *Journal of Integrative Environmental Sciences,* vol. 16, no. 1, pp. 191-207, 2019, doi: 10.1080/1943815x.2019.1707233.

[15] S. Dhib, C. M. Mannaerts, Z. Bargaoui, V. Retsios, and B. H. P. Maathuis, "Evaluating the MSG satellite Multi-Sensor Precipitation Estimate for extreme rainfall monitoring over northern Tunisia," (in English), *Weather and Climate Extremes,* vol. 16, pp. 14-22, Jun 2017, doi: 10.1016/j.wace.2017.03.002.

[16] D. S. Wilks, *Statistical Methods in the Atmospheric Sciences*. 2006, pp. 627-627.

[17] W. Roberts, G. P. Williams, E. Jackson, E. J. Nelson, and D. P. Ames, "Hydrostats: A Python Package for Characterizing Errors between Observed and Predicted Time Series," *Hydrology,* vol. 5, no. 4, 2018, doi: 10.3390/hydrology5040066.

[18] H. V. Gupta, H. Kling, K. K. Yilmaz, and G. F. Martinez, "Decomposition of the mean squared error and NSE performance criteria: Implications for improving hydrological modelling," *Journal of Hydrology,* vol. 377, no. 1-2, pp. 80-91, 2009, doi: 10.1016/j.jhydrol.2009.08.003.

[19] H. Kling, M. Fuchs, and M. Paulin, "Runoff conditions in the upper Danube basin under an ensemble of climate change scenarios," *Journal of Hydrology,* vol. 424-425, pp. 264-277, 2012, doi: 10.1016/j.jhydrol.2012.01.011.

[20] M. W. Kimani, J. C. B. Hoedjes, and Z. B. Su, "An Assessment of Satellite-Derived Rainfall Products Relative to Ground Observations over East Africa," (in English), *Remote Sensing,* vol. 9, no. 5, May 2017, doi: ARTN 430 10.3390/rs9050430.

[21] M. Maranan, A. H. Fink, P. Knippertz, L. K. Amekudzi, W. A. Atiah, and M. Stengel, "A Process-Based Validation of GPM IMERG and Its Sources Using a Mesoscale Rain Gauge Network in the West African Forest Zone," (in English), *Journal of Hydrometeorology,* vol. 21, no. 4, pp. 729-749, Apr 2020, doi: 10.1175/jhm-d-19-0257.1.

[22] C. C. Funk *et al.*, "Introducing and Evaluating the Climate Hazards Center IMERG with Stations (CHIMES) Timely Station-Enhanced Integrated Multisatellite Retrievals for Global Precipitation Measurement," (in English), *Bulletin of the American Meteorological Society,* vol. 103, no. 2, pp. E429-E454, Feb 2022, doi: 10.1175/Bams-D-20-0245.1.